Characterization of GX 339-4 outburst of 2010-11: analysis by xspec using two component advective flow model

Dipak Debnath[1]⋆, Santanu Mondal[1], Sandip K. Chakrabarti[1,2]

[1] *Indian Centre For Space Physics, 43 Chalantika, Garia Station Road, Kolkata, 700084, India*
[2] *S. N. Bose National Center for Basic Sciences, JD-Block, Salt Lake, Kolkata, 700098, India*

ABSTRACT

We study spectral properties of GX 339-4 during its 2010-11 outburst with Two Component Advective Flow (TCAF) model after its inclusion in XSPEC as a table model. We compare results fitted by TCAF model with combined disk black body and power-law model. For a spectral fit, we use $2.5 - 25$ keV spectral data of the PCA instrument onboard RXTE satellite. From our fit, accretion flow parameters such as Keplerian (disk) rate, sub-Keplerian (halo) rate, location and strength of shock are extracted. We quantify how the disk and the halo rates vary during the entire outburst. We study how the halo to disk accretion rate ratio (ARR), quasi-periodic oscillations (QPOs), shock locations and its strength vary when the system passes through *hard, hard-intermediate, soft-intermediate*, and *soft* states. We find pieces of evidence of monotonically increasing and decreasing nature of QPO frequencies depending on the variation of ARR during rising and declining phases. Interestingly, on days of transition from hard state to hard-intermediate spectral state (during the rising phase) or vice-versa (during decline phase), ARR is observed to be locally maximum. Non-constancy of ARR while obtaining reasonable fits points to the presence of two independent components in the flow.

Key words: accretion, accretion discs – radiation: dynamics – black hole physics – shock waves – stars:individual: GX 339-4 – X-Rays: binaries

1 INTRODUCTION

Galactic transient black hole candidates (BHCs) are very interesting objects to study in X-rays because they exhibit rapid evolutions in their temporal and spectral properties during outbursts (see for reviews, Remillard & McClintock 2006; McClintock & Remillard 2006). In the past two decades, especially after the launch of *Rossi X-ray Timing Explorer* (RXTE), our understanding of black hole binaries has improved significantly. However, real progress in extracting physical parameters was hampered due to lack of appropriate data analysis software. For instance, fitting a spectrum with a black body and a power-law component (so-called diskbb plus power-law, or compST models in XSPEC) tells us that there is a multicolor soft photon source such as a Shakura-Sunyaev standard disk (Shakura & Sunyaev 1973, hereafter SS73) and a so-called Compton cloud (Sunyaev & Titarchuk 1980, 1985) which is a hot region of free electrons with certain optical depth and temperature. However, cause of formation of the standard disk, nature and origin of Compton cloud or a specific spectral state remained missing. There was no information about why and how optical depths and temperatures of the cloud or the accretion rates of the disk vary.

A turning point in theoretical solutions of viscous transonic accretion flows around black holes (Chakrabarti 1990a,b, 1996) came when it was shown that flows above a critical viscosity parameter α will become a Keplerian disk, while those below will remain sub-Keplerian. This fact was used to construct a two component advective flow (TCAF) model (Chakrabarti & Titarchuk 1995, hereafter CT95; Ebisawa, Titarchuk & Chakrabarti 1996; Chakrabarti 1997, hereafter C97), which not only explains under what circumstances a standard Keplerian disk could form, but also explains state transitions and variation of flow parameters during outbursts of several black holes reasonably well (Debnath et al. 2008, 2013; Dutta & Chakrabarti 2010; Nandi et al. 2012). In a TCAF solution, low viscosity and low angular momentum matter piles up behind a centrifugal barrier forming an axisymmetric shock (C90a,b; Molteni et al., 1994; Ryu et al. 1997), which is by and large stable even under non-axisymmetric perturbations (Okuda et al. 2007). This barrier is known as the 'CENtrifugal pressure dominated BOundary Layer', or CENBOL and acts as the Compton cloud. Regions of higher viscosity forms a Keplerian disk which settles down to a standard Shakura-Sunyaev disk when the cooling is efficient (see, Giri & Chakrabarti 2013; Giri, Garain & Chakrabarti 2014, and references therein). Soft photons from SS73 disk are inverse Comptonized by the post-shock region (CENBOL) to form

⋆ E-mail: dipak@csp.res.in

hard photons and thus in the TCAF (CT95) solution a separate Compton cloud is not required. Another novel aspect is that fitting with TCAF does not require explicit knowledge of viscosity parameter. TCAF directly uses two accretion rates, one for high viscosity flow (for super-critical viscosity parameter α), namely, standard SS73 like Keplerian component (disk), and the other for low viscosity flow (sub-critical α), namely, sub-Keplerian (low angular momentum) component (halo). Location and strength of shocks which TCAF uses also depend on viscosity, but since we use them as fitting parameters, a prior knowledge of viscosity is not essential. Furthermore, low-frequency quasi-periodic frequencies (QPOs) are supposed to be due to oscillations of the CENBOL region from where jets are originated (Chakrabarti 1999). So a separate oscillating component is not required to explain QPOs. Non-thermal electrons are produced by the shock which may produce long power-law tail (Chakrabarti & Mandal 2006) obviating the need to inject non-thermal electrons externally (Zdziarski et al. 2001). Thus, TCAF aims to resolve all the spectral and temporal properties along with disk-jet connections within the framework of a single solution. These advantages motivated us to fit spectral data from BHCs with TCAF (Debnath, Chakrabarti & Mondal 2014; Mondal, Debnath & Chakrabarti 2014a), even when they may be fitted equally well with other available models (such as diskbb plus power-law) in XSPEC. Other models do not discuss origin of the Compton cloud or corona (Haardt & Maraschi 1993; Zdziarski et al. 2003) and do not unify timing properties (e.g., QPOs) with spectral properties or obtain outflow rates with spectral properties as TCAF does. Unlike a persistent source, where accretion rates could be stable for a long time, in an outburst source, rates have to be varying. One of the most natural ways to achieve this is by varying viscosity. It is possible that an outburst may be triggered by enhancement of viscosity at the outer disk. Mandal & Chakrabarti (2010) suggested that enhanced viscosity redistributes part of halo (i.e., low angular momentum flow) into a SS73 like Keplerian flow, keeping the total mass-flow rate roughly constant. Their conclusion was that the accretion rate of the disk must go up rapidly due to enhanced viscosity before coming down when viscosity is reduced again. This conversion and formation of TCAF configuration has been demonstrated recently by numerical simulations Giri & Chakrabarti (2013). A sudden increase in viscosity at the outer edge would progressively shift inner edge of the Keplerian disk towards the black hole which causes a enhancement of soft luminosity. Declining phase starts when the source of enhanced viscosity is removed and there is a resulting shortfall of Keplerian component. Thus fitting an outburst source data with TCAF having two evolving accretion rates, shock location (CENBOL boundary) and shock strength may give us insight into how the disk structure really evolves. As mentioned earlier, though enhanced viscosity and its temporal and spatial variations are believed to be the prime cause of the outburst, no prior knowledge of viscosity is required since the fitting parameters carry those information. In future, we would pursue to derive even more fundamental parameters, such as, specific energy and angular momentum distribution inside the flow and then computation of viscosity would be possible.

Galactic transient black hole candidate (BHC) GX 339-4 was first observed in 1973 (Markert et al. 1973) by $1 - 60$ keV MIT X-ray detector onboard OSO-7 satellite. This stellar-mass black-hole binary has a mass function of $M_{bh} \, sin(i) = 5.8 \pm 0.5 \, M_{\odot}$ and low-mass companion of mass $m = 0.52 \, M_{\odot}$ (Hynes et al. 2003, 2004). This binary system is located at a distance of $d \geqslant 6$ kpc (Hynes et al. 2003, 2004) with R.A.$=17^h02^m49^s.56$

and Dec.$=-48°46'59''.88$. This recurring transient source has undergone five X-ray outbursts (Nowak et al. 1999; Belloni et al. 2005; Nandi et al. 2012) during the RXTE era (in the period from 1996 to 2011). Based on evolution of their spectral and timing properties (McClintock & Remillard 2006; Belloni et al. 2005; Remillard & McClintock 2006; Debnath et al. 2013) which are also found to be correlated with a characteristic temporal evolution, namely, hardness-intensity diagram (HID) (Maccarone & Coppi 2003; Homan & Belloni 2005), various spectral states are identified during the past outbursts of the same source. In general, there are mainly four basic states - *hard, hard-intermediate, soft-intermediate*, and *soft* states are observed during an outburst (Homan & Belloni 2005; Debnath et al. 2013; Motta et al. 2009; Nandi et al. 2012). In the literature, one can find extensive discussions on the properties of these spectral states (van der Klis 2004; Belloni et al. 2005; Remillard & McClintock 2006; Debnath et al. 2008, 2013). Complex outburst profile of BHCs begins and ends in hard/low hard state, keeping soft and intermediate states in between. It has been pointed out (Nandi et al. 2012; Debnath et al. 2013) that these four basic spectral states form a hysteresis loop during their outburst phases in the sequence of *hard → hard-intermediate → soft-intermediate → soft → soft-intermediate → hard-intermediate → hard*. According to TCAF, hard states are formed when soft photons are unable to cool the Compton cloud (comprising collectively of CENBOL, pre-shock halo and outflow) while reverse is true for soft states. Intermediate states are a proof that accretion rates are comparable and they occur when viscosity is either rising or declining (see also, Dutta & Chakrabarti 2010).

GX 339-4 showed X-ray activity of 17 mCrab (in $4 - 10$ keV), observed on 2010 January 03 with the MAXI/GSC onboard ISS (Yamaoka et al. 2010). The source remained active in X-rays for the next ~ 14 months and during this period, the source was monitored with RXTE, starting from 2010 January 12 (Tomsick 2010). Temporal and spectral properties of the source was studied extensively during this outburst by several authors (Motta et al. 2011; Stiele et al. 2011; Shidatsu et al. 2011a; Debnath et al. 2010, hereafter Paper I; Nandi et al. 2012, hereafter Paper II). Several attempts were made to explore multi-wavelength properties of the source during this outburst (Rahoui et al. 2012; Buxton et al. 2012; Dincer et al. 2012; Cadolle et al. 2012). Temporal as well as spectral variabilities and radio jets are observed during this outburst (Corbel et al. 2013a,b; Yan & Yu 2012). In *Paper I*, a preliminary result of timing and spectral properties during initial rising phase was presented. Subsequently, in *Paper II*, detailed timing and spectral study during the entire outburst was presented. In both these papers, spectral properties were studied with a combination of conventional thermal (disk black body) and non-thermal (power-law) model components. In order to understand detailed accretion flow dynamics, we need to fit with a more physical model, such as TCAF, which would enable us to extract actual physical parameters of the accretion flow.

In this *paper*, for the first time, we show results of implementation of TCAF model in HEASARC's spectral analysis package XSPEC. Our goal is to find how the flow parameters vary from the beginning to the end of the outburst of GX 339-4 during its recent 2010-11 episode.

Since the number of available RXTE/PCA archival data points is too high, we choose a total of 50 observations spread over 419 days of the entire outburst, starting from 2010 January 12 to 2011 March 6. We also compare our fitted spectral results with that of the conventional combined disk black body (DBB) and power-law (PL) model presented in Paper II. From our current study, we ob-

tain variations of the flow parameters for the same states, namely, *hard, hard-intermediate, soft-intermediate*, and *soft* as described in Paper II. Here, we mainly concentrate on the rising and the declining phases of the outburst, where state transitions occur. From the TCAF model fitted $2.5 - 25$ keV PCA spectra, we find that the variations of DBB and PL fluxes during the outburst as observed by Nandi et al. (2012) are consistent with variations of Keplerian (disk) rate and sub-Keplerian (halo) rate respectively. We find some intriguing properties of the variation of *accretion rate ratio* (ARR, i.e., ratio between sub-Keplerian halo and Keplerian disk rates) and frequencies of quasi-periodic oscillations (LFQPOs; if observed) during the days of class transitions. These will be discussed below and require further investigations.

The *paper* is organized in the following way: in the next Section, we present a briefly describe the TCAF solution and how a spectrum is generated. In §3, we discuss observational results and data analysis procedures using HEASoft software. Here, we also mention methods of generation of TCAF model *fits* file used for spectral fittings. In §4, we present spectral analysis results obtained from TCAF model fits of RXTE PCA data and compare results with that of the combined DBB and PL model fits. We note special behaviour of the extracted flow properties when the object is in different spectral states, with a particular emphasis during state transitions. Finally, in §5, we present a brief discussion of our results and make concluding remarks.

2 MODEL DESCRIPTION AND GOVERNING EQUATIONS

A brief description of Two Component Advective Flow (TCAF) solution has been given in the Introduction. We use Chakrabarti-Titarchuk (1995; CT95) model code as the basic program for generating v0.1 of TCAF model *fits* file to fit black hole spectra. In the TCAF solution, an SS73 like Keplerian disk (high viscosity component) at the equatorial plane is immersed inside a low angular momentum sub-Keplerian (low viscosity) halo. The flow is considered to be axisymmetric. Though accretion rates would be a function of radial distance in a rapidly evolving system such as an outburst (Dutta & Chakrabarti 2010), each observational result is fitted with an effective accretion rate. The Keplerian disk, truncated at the shock location, locally emits a flux of radiation same as that produced by an SS73 disk. Geometry around the black hole is described by Paczyński & Witta (1980) pseudo-Newtonian potential $\Phi_{PN} = -\frac{1}{2(r-1)}$, where r is the radial distance of the flow in units of Schwarzschild radius ($r_g = 2GM_{BH}/c^2$, c being the velocity of light and M_{BH} being the mass of the black hole). As a black hole accretion is necessarily transonic (e.g., Paczyński & Bisnovatyi-Kogan 1981; Paczyński & Witta 1980; Chakrabarti 1990a, hereafter C90a), for a large region of the parameter space, the flow must jump from supersonic to subsonic branch, forming a standing or oscillating shock (C89; C90a,b) before entering into a black hole through the inner sonic point. CT95 considers the region between the shock to inner sonic point, namely, the post-shock region (CENBOL), to be the Compton cloud. Contribution of the pre-shock halo, or winds were separately discussed there. In the present fits file, we do not include effects of optically thin pre-shock halo and the outflowing matter. The CENBOL cools down through inverse Comptonization and produces observed hard photons. Thus very cold CENBOL does not produce hard photons or outflows at all. (Chakrabarti 1999; Singh & Chakrabarti 2011, and references therein). In CT95

spectral properties are studied using only strong shocks since the idea there was to show that TCAF could explain spectral state transitions, in principle. Spectrum was generated for a set of Keplerian (disk) rates, sub-Keplerian (halo) rates and shock locations. Unlike other models (Zdziarski et al. 2003, and references therein), TCAF does not require to add an extra 'reflection' component, since this component is in built into the procedure. Albedo at each disk radius is included in computing disk reflection. Spectrum is calculated from intercepted photons by CENBOL region. Fraction of absorbed hard X-rays by the pre-shock Keplerian disk is used to heat it up and emit blackbody radiation at a higher temperature. The procedure is iterated till a convergence in all parameters is achieved. As given in CT95, we computed the effect by taking into account the photoelectric absorption and recoil effects. We took care of contribution of the first scattering exactly and of the multiple scattering using Fokker-Planck diffusion approximation (Sobolev 1975).

In an outburst, the shock is expected to have a time varying compression ratio R, since the post-shock region is expected to cool down as accretion rate increases. This, in turn, is governed by enhancement of viscosity. Thus, we use R as a parameter. R determines post-shock density (radial optical depth) and post-shock temperature, which, together with an assumption of vertical equilibrium gives height $h(X_s)$ (in r_g) of the flow at the shock X_s (in r_g), an important quantity which determines percentage of soft photons intercepted by the 'Compton cloud'. Flux F_{ss} emitted from the optically thick Keplerian disk is obtained from SS73,

$$F_{ss} = 6.15 \times 10^8 \dot{M} r^{-3} \Im (\frac{M_{BH}}{M_\odot})^{-2} \; ergs \; cm^{-2} s^{-1}. \qquad (1)$$

Here, $\Im = (1 - 3/r)^{1/2}$. In the above equation, mass of the black hole M_{BH} is measured in units of mass of the Sun ($M_\odot$), disk accretion rate $\dot{M}$ is in units of $gm \; s^{-1}$. Although this equation was derived with a no-torque condition at the inner stable circular orbit (ISCO) at $r = 3$, it remains the same in our case, even though our SS73 disk is effectively evaporated inside the CENBOL and mixes with the sub-Keplerian flow when CENBOL is hot enough (in hard states). In soft states, the CENBOL itself is cold and Keplerian disk can reach close to ISCO. Shidatsu et al. (2011b), calculated innermost disk radius for the black hole candidate GX 339-4, which is consistent with the accepted picture of the high/soft state in which standard disk may always extend up to ISCO. However, Allured et al. (2013) examined inner disk radius using different models (e.g., thermal and relativistic line broadening etc.) at different luminosities in the hard states and found that the disk need not go up to ISCO. In fact, since a black hole accretion is always supersonic, a Keplerian disk will be almost sonic/transonic at ISCO to prepare itself for the final plunge into the horizon with a radial velocity same as that of the velocity of light. So, disk extending up to ISCO is always an assumption, more so for low accretion rates. This is also evident from viscose transonic flow solutions (C90ab). Angular momentum is transported inside the CENBOL till the inner sonic point at $r_c \sim 2.5 r_g$ (see, Chakrabarti 1990a), where, ideally a torque-free condition should be applicable. Inside r_c, angular momentum transport is negligible. In future, we plan to actually simulate Keplerian disk along with the halo and compute time dependent spectra and several assumptions made here would become unnecessary. Already we have reported preliminary results of our simulations (Giri & Chakrabarti 2013; Giri, Garain & Chakrabarti 2014). In the simulation, temperature would be obtained from the global solution of an advective flow, and not as in SS73 where local gravitational energy dissipation was used.

The post-shock region becomes hot due to conversion of ki-

netic energy of the pre-shock flow into thermal energy. However, electrons lose energy due to bremsstrahlung and Comptonization of soft photons emitted from the Keplerian disk. Energy equation which protons and electrons obey in the post-shock region is given by (CT95),

$$\frac{\partial(\varepsilon + \frac{P}{\rho})}{\partial r} + (\Gamma - \Lambda) = 0, \tag{2}$$

where, specific energy (Chakrabarti 1989) of the flow is given by,

$$\varepsilon = \frac{v^2}{2} + na^2 + \frac{\lambda^2}{2r^2} - \frac{1}{2(r-1)}, \tag{3}$$

and Γ and Λ are the heating and the cooling terms, respectively. Here, λ is the specific angular momentum in units of cr_g, v is infall velocity in units of c, $n = \frac{1}{(\gamma-1)}$ is polytropic index, $a = \sqrt{(\frac{\gamma P}{\rho})}$ is the sound speed of the medium in units of c, and γ is adiabatic index. Equation (2) was not used in pre-shock halo region. Synchrotron radiation was not used in the present version of our fits file.

Since temperature and height of the post-shock region depend on the shock location and strength, it is more physical to write them as functions of flow parameters. For this, we use pressure balance condition, where sum of the thermal pressure and the ram pressure must match on both sides of the shock (Landau & Lifshitz 1959). In pressure balance condition (C89), we assume that the pre-shock flow is cooler, $a \sim 0$ as it falls freely and $X_s^2 \gg \lambda^2$. Using adiabatic a, we get height of shock front as, $h_{shk} = a \, X_s^{0.5} \, (X_s - 1)$ for vertical equilibrium model. Initial guess of the shock temperature is obtained from the definition $a_s^2 = \frac{\gamma k T_{shk}}{\mu m_p}$. Thus, temperature ($T_{shk}$) and height ($h_{shk}$) of the shock becomes:

$$T_{shk} = \frac{m_p(R-1)c^2}{2R^2 k_B(X_s-1)}, \tag{4}$$

$$h_{shk} = \sqrt{\left(\frac{\gamma(R-1)X_s^2}{R^2}\right)}, \tag{5}$$

where, m_p, R, k_B and X_s are mass of the protons, compression ratio, Boltzmann constant and shock location of the flow respectively. Soft photons from the pre-shock Keplerian disk are intercepted by the hot CENBOL. As the accretion rate increases, number of scattering increases and photons gain more energy while cooling down the CENBOL. Details about the solution procedure and enhancement factor calculation due to Comptonization is in Eq. (12a-14) of CT95. The outcome depends on the opacity,

$$\tau_T = \int_{r_i}^{X_s} \sigma_T n_e dr. \tag{6}$$

Here, r_i is the inner radius of CENBOL $\sim 2.5r_g$. Average energy exchange per scattering is given by ($h\nu, kT_e \ll m_e c^2$),

$$\frac{\Delta\nu}{\nu} = \frac{4kT_e - h\nu}{m_e c^2}. \tag{7}$$

When $h\nu \ll kT_e$, photons gain thermal energy. Here, terms n_e, σ_T, T_e and r_i used in above two equations are number density of electrons in the post-shock region, Thomson scattering cross-section, average temperature of electrons and inner edge of the flow respectively. Balance of scattering and energy gain of photons give the power-law distribution as,

$$F_\nu \propto \nu^{-\alpha}. \tag{8}$$

As mentioned already, to generate the model spectra (which are used as inputs for generating TCAF model *fits* file), we made several modifications in original CT95 code to include,

i) Variation of compression ratio R is allowed from 4 (strong) to 1 (weak). CT95 assumed only strong shock for illustration purpose.

ii) Computation of temperature of post-shock region using this R.

iii) Radial velocity of a rotating flow as in C97.

iv) Spectral hardening correction of Shimura & Takahara (1995), which depends on the accretion flow rate. We uniformly consider the correction factor (*f*) to be 1.8 to calculate effective temperature in emitted spectrum.

We wish to mention certain limitations of the present version: although by taking extreme limits of Keplerian rate ($\dot{m}_d$ in Eddington rate) or sub-Keplerian rate ($\dot{m}_h$ in Eddington rate) as close to zero as possible, we could have extreme hard or soft states, these limits require finer model grids. In the present version (v0.1), we do not consider cases with $\dot{m}_h \to 0$ (soft states). However, cases with $\dot{m}_d \to 0$ are not needed as spectral index is highly insensitive to $\dot{m}_d$ near this limit (Ebisawa, Titarchuk & Chakrabarti 1996). We also do not consider bulk motion Comptonization (see, CT95; Titarchuk & Zannias 1998). Present model of TCAF does not include magnetic fields explicitly or production of non-thermal photons by the shock. Thus inverse Comptonization of non-thermal photons produced in the post-shock region could not be included and thus some features which may occur at much higher energies in different sources (Zdziarski et al. 2001; Chakrabarti & Mandal 2006) cannot be fitted with the current *fits* file. All these points will be taken up in future.

3   OBSERVATION AND DATA ANALYSIS

We present spectral analysis results of publicly available archival data from RXTE Proportional Counter Array (PCA) instrument for entire 2010-11 outburst of GX 339-4, starting from 2010 January 12 (Modified Julian date, MJD=55208) to 2011 March 6 (MJD=55626) from the PCA (Jahoda et al., 1996). In general, we follow the same analysis techniques as discussed in Paper II, for extraction of source and background '.pha' files using *Standard2* mode science data of PCA (FS4a*.gz). $2.5 - 25$ keV PCA background subtracted spectra are fitted with TCAF model *fits* file in XSPEC v. 12.8. To achieve the best fit, a Gaussian line of peak energy around 6.5 keV (iron-line emission) is used. For the entire outburst, we keep hydrogen column density (N_H) for absorption model *wabs* fixed at 5×10^{21} atoms cm^{-2} (Motta et al. 2009) and assume a 1.0% systematic error. After achieving the best fit based on reduced chi-square (χ_{red}^2) value ($\leqslant 2$), to find 90% confidence error values for TCAF model fitted parameters, 'err' command is used (except data for rising soft-intermediate and soft states, from MJD = 55316 to MJD = 55593, 1 σ error are given, since here reduced χ^2 values are found to be in between $1.8 - 2.8$). In Appendix I, detailed spectral fitted analysis results with observed QPO frequencies are provided (Note that error values for TCAF model fitted parameters which are given in Appendix I, are average values of 90% confidence ± error, or, 1 σ error).

One can also fit a spectrum by manually comparing observational spectrum with the theoretical model spectra, generated by different input parameters in TCAF model source code (Dutta & Chakrabarti 2010). However, in order to fit spectra more accurately one needs to use it in a complete package like XSPEC, which automatically achieves the best fit by iterative least square fit technique. From the spectral fit, one can obtain model fitted values of reduced chi-square, degrees of freedom, parameter errors etc. In order to fit black hole spectra with the TCAF model in XSPEC,

Table 1. TCAF model *fits* files generated with different sets of model input parameter grids

Set	M_{BH} ($M_\odot$)			$\dot{m}_d$ ($\dot{M}_{Edd}$)			$\dot{m}_h$ ($\dot{M}_{Edd}$)			X_s (r_g)			R		
	Min	Max	GN	Min	Max	GN	Min	Max	GN	Min	Max	GN	Min	Max	GN
I	3	15	6	0.1	12.1	18	0.1	12.1	18	6	456	20	1	4	10
II	3	15	6	0.1	2.0	15	0.1	2.0	15	6	456	24	1	4	12
III	3	15	6	2.0	12.1	15	2.0	12.1	15	6	456	24	1	4	12
IV	3	15	6	0.1	2.0	12	0.1	12.1	20	6	456	24	1	4	12
V	3	15	6	0.1	12.1	20	0.1	2.0	12	6	456	24	1	4	12

Here Min, Max, and GN represent minimum, maximum and grid numbers for logarithmic equi-spaced model input parameters.

we have generated model *fits* file (*TCAF0.1.fits*) using theoretical spectra generated by varying five input parameters in CT95 code (after modifications mentioned earlier) and included it in XSPEC as an additive table model. These parameters are: *i*) black hole mass (M_{BH}) in solar mass ($M_\odot$) unit, *ii*) Keplerian rate ($\dot{m}_d$ in Eddington rate, $\dot{M}_{Edd}$), *iii*) sub-Keplerian rate ($\dot{m}_h$ in $\dot{M}_{Edd}$), *iv*) location of shock (X_s in Schwarzschild radius r_g), and *v*) compression ratio (*R*) of the shock. Of course, the model normalization value (*norm*), which for simplicity could be written as $\frac{R_z^2}{4\pi D^2} sin(i)$, where, '$R_z$' is the effective height of the Keplerian component in *km* at the pre-shock region, '*D*' is source distance in 10 kpc unit and '*i*' is disk inclination angle with the line of sight is also a variable. However, since R_z need not come out of SS73 model due to its proximity of the shock surface, we leave it as a free parameter to be determined from the best fitted value, very much like R_{in}, the inner edge of the disk, as obtained from the normalization of the diskbb model fits. In future, when we have a clearer picture of how R_z should be computed theoretically, we will create a fits file with this to be the sixth parameter.

Five model input parameters mentioned above were varied in the following ranges: *i*) M_{BH}: 3 -15 $M_\odot$, *ii*) $\dot{m}_d$: 0.1 - 12.1 $\dot{M}_{Edd}$, *iii*) $\dot{m}_h$: 0.1 - 12.1 $\dot{M}_{Edd}$, *iv*) X_s: 6 - 456 r_g, and *v*) R: 1 - 4, respectively. We first generate $\sim 4 \times 10^5$ model spectra by varying input parameters in above mentioned limits and then these model spectra are used as input files to a program written in FORTRAN, to generate a crude grid based model *fits* file (Set I of Table 1). However, once a reasonable fit is obtained with this *fits* file, spectra are refitted with appropriate finer grid based *fits* file (Set II-V of Table 1), to have a better fit with minimum parameter error values as well as better reduced χ^2. This two step process is presently needed as we do not have a very fine grid for the entire parameter space. When we build the model with final grids around $\dot{m}_h \rightarrow 0$ also, fitting of soft states would be addressed satisfactorily. In the fitted results below, we froze the mass to be 5.8 and therefore only four parameters were varied.

4 RESULTS OF FITTING OF DATA BY TCAF SOLUTION

Detailed temporal and spectral properties of the source during its 2010-11 outburst is already presented by several authors (Motta et al. 2011; Stiele et al. 2011; Shidatsu et al. 2011a; Cadolle et al. 2012, Paper I and Paper II).

Presently, we fit with *TCAF0.1.fits* file as generated above and compare our spectral results with combined DBB and PL model fitted results presented in Paper II. Here we discuss how the flow parameters evolve during rising and declining phases of the outburst.
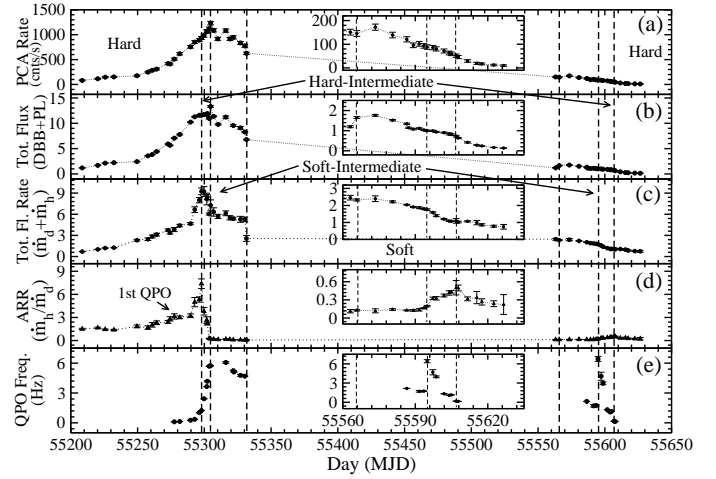
Figure 1. Variation of (a) $2 - 25$ keV PCA count rates (cnts/sec), (b) combined disk black body (DBB) and power-law (PL) model fitted total spectral flux in $2.5 - 25$ keV range (in units of 10^{-9} $ergs$ cm^{-2} s^{-1}), (c) TCAF model fitted total flow (accretion) rate (in $\dot{M}_{Edd}$; sum of Keplerian disk, $\dot{m}_d$ and sub-Keplerian halo $\dot{m}_h$ rates) in the $2.5 - 25$ keV energy band, and (d) Accretion Rate Ratio (ARR; ratio between halo and disk rates) with day (MJD) for the 2010-11 outburst of GX 339-4 are shown. In the bottom panel (e), observed primary dominating QPO frequencies (in Hz) with day (MJD) are shown. The vertical dashed lines indicate the transitions of between different spectral states. Zoomed quantities in the decay phase are in the inset.

Detailed analysis results are given in Table Appendix I, where we present Observations IDs (Col. 2), date of observation (Col. 3), accretion rates (Cols. 4-5), accretion rate ratios (Col. 6), shock locations (Col. 7), Compression Ratios (Col. 8), shock heights (Col. 9), temperature at the CENBOL surface from Eq.(4) (Col. 10), thickness R_z of the pre-shock Keplerian disk in km (Col. 11), line width and line depths (Cols. 12-13) of the iron line (where applicable), QPO frequencies (Col. 14) and finally χ^2/DOF (Col. 15).

4.1 Evolution of fitted parameters during the outburst

In Fig. 1a, variation of background subtracted RXTE PCA count rate in $2 - 25$ keV ($0 - 58$ channels) energy band with day (MJD) is shown. In Figs. 1b & 1c, variations of combined DBB and PL model fitted total spectral flux (flux contributions for the DBB and PL model components are calculated by using the convolution model 'cflux' technique after fitting a spectrum with combined model components) in $2.5 - 25$ keV energy band (Paper II) and TCAF model fitted total accretion rates (combined Keplerian disk and sub-Keplerian halo rates) in the same energy band with day (MJD) are shown. In Fig. 1d, variation of *Accretion Rate Ratio* ARR (defined as the ratio of sub-Keplerian halo $\dot{m}_h$ and Keplerian disk $\dot{m}_d$ rates) with day (MJD) is shown. As will be evident from the plots of Fig. 3, it may be better to treat ARR as a proxy to hardness ratio since the latter is not a black hole mass independent concept. We also zoom a part of ARR plot in the declining phase to see their behaviour clearly and to emphasize that it reaches a maximum on the day when the hard state starts. Observed QPO frequencies are shown in Fig. 1e. From the variation of ARR and nature (shape, frequency, *Q* value, rms% etc) of QPO (when observed) in the four different spectral states, namely, *hard, hard-intermediate, soft-intermediate, soft*, we find a distinct pattern. On or about the days of spectral transitions between states as reported

in Paper II (marked with vertical dashed lines in Figs. 1-3), ARR shows interesting behaviour (to be discussed in detail below). We also see that TCAF model holds good in fitting the spectra (model fitted χ^2_{red} varies $\sim 0.9 - 1.6$) from hard, hard-intermediate and soft-intermediate (declining) spectral states. In rising soft-intermediate and soft spectral states, TCAF model fitted χ^2_{red} varies in the range $\sim 1.8 - 2.8$. However, for a soft spectral state, where the source stayed for almost ~ 8 months, TCAF model cannot be used since we essentially need a single component with a high rate (outside of our grid used in this fits file). In future, we will generate model *fits* file with a larger parameter range including $\dot{m}_h \rightarrow 0$, high $\dot{m}_d \geqslant 12$ and bulk motion Comptonization. In Fig. 2(a-e), variations of TCAF model fitted shock parameters, namely, T_{shk} in 10^{10} K, and X_s in units of r_g, h_{shk} in units of r_g, the ratio h_{shk}/X_s and R are shown as a function of time (MJD). During the initial rising phase of the outburst, as the day progresses, the shock generally moves towards the black hole (see, Fig. 2b) while progressively becoming weaker (see, Fig. 2e) due to increasing cooling. At the same time, shock height (h_{shk}) and temperature (T_{shk}) increase initially, then start to decrease gradually (Fig. 2 c-d) . The ratio of shock height and shock location is around 0.7 for a long interval of time when the object was in a hard state to about $0.3-0.4$ in the soft state. Thus the geometry of the CENBOL is sometimes spherical and sometimes disk like as far as Comptonization process goes. So, we use Eq. (9) of Hua & Titarchuk (1995) which is valid for two regimes to obtain spectral index. To obtain an average temperature of the CENBOL, we took weighted average of the temperature variation assuming it to be spherical. The processes followed are exactly as in CT95.

In the declining phase, almost an opposite nature of variations of these four parameters are observed. In Fig. 3(a-b), variations of combined DBB and PL model fitted DBB flux (top panel) and TCAF model fitted Keplerian disk rate $\dot{m}_d$ with day (MJD) are shown. Similarly, in Fig. 3(c-d), variations of combined DBB and PL model fitted PL flux and TCAF model fitted sub-Keplerian halo rate $\dot{m}_h$ (bottom panel) with day (MJD) are shown. Observed variations of these two different types of model fitted fluxes/rates are similar in nature.

Note that the pre-shock Keplerian disk thickness R_z which comes out from the fit (Col. 11) is not necessarily decreasing with the reduction of the shock. This is because the increase in accretion rate caused radiation pressure to increase which puffs up the inner disk.

4.2 Evolution of spectral and temporal properties during the outburst

In Figs. 4(a-f), TCAF model fitted 2.5 – 25 keV background subtracted PCA spectral flux, $E^2 f(E)$ in units of keV^2 (*Photons cm^{-2} s^{-1} keV^{-1}*) with variation of $\Delta\chi$ in three different (hard, hard-intermediate, soft-intermediate) spectral states in both rising and declining phases are shown. These results are presented in Table 'Appendix I'.

Generally, low frequency quasi-periodic oscillations (LFQ-POs) in $\sim 0.01 - 30$ Hz are observed during hard and intermediate spectral states of transient black hole candidates (see, Remillard & McClintock 2006, for a review). From detailed temporal and spectral study (using a combined DBB and PL model fits) of present 2010-11 outburst of GX 339-4 (Paper I and Paper II) and 2010 & 2011 outbursts of H 1743-322 (Debnath et al. 2013), it has been observed that QPO frequency increases monotonically during rising hard and hard-intermediate spectral states, and decreases monotonically through the same spectral states in declining phases.
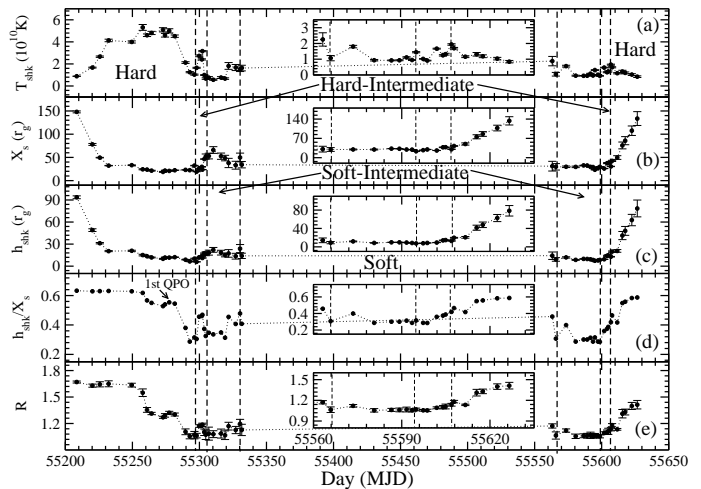
Figure 2. Variation of TCAF model fitted/derived shock (a) temperature (T_{shk} in 10^{10} K), (b) location (X_s in r_g), (c) height (h_{shk} in r_g), (d) ratio between h_{shk} & X_s, and (e) compression ratio (R) with day (MJD) are shown. The shock height and temperature are calculated using Eqs. 4 & 5 respectively.

It has also been observed that during soft-intermediate spectral states of both rising and declining phases, QPOs are observed sporadically, whereas no LFQPOs are observed in the soft spectral state. According to Paper II and Debnath et al. (2013), maximum value of evolving QPO frequencies (fitted with Propagating Oscillatory Shock (POS) model solution) are observed on the final day of rising hard-intermediate spectral state *and* on the very first day of the same spectral state in declining phase of outburst. From our spectral study of present outburst of GX 339-4 using TCAF model, we notice that on these days when the observed QPO frequency is maximum, ARR reaches its lower values, where source stayed for a longer durations (in soft-intermediate or soft spectral states) with little change in the rising or releases from from its long stayed Keplerian disk dominated lower values to increase rapidly in the declining phases of the outburst (Fig. 1d-e). It also has been noticed that during the rising phase of the outburst, QPO frequency starts to increase rapidly when ARR reaches its peak value and during the declining phase QPO frequency starts to decrease slowly (or leaves its rapid decrease phase) when ARR reaches its maximum value (of the declining phase) of the outburst (Fig. 1d-e).

In Papers I & II, spectral classifications were discussed based on the degree of importance of DBB and PL model components (according to variation of fitted component values and their individual fluxes) and nature (shape, frequency, Q value, percentage of rms amplitude etc.) of QPO (if present). However, here we find that ARR varies in a well defined way in these states. In the rising phase, ARR increases steadily in the hard state, decreases very fast in the hard intermediate state, remains almost constant in the soft-intermediate state. Exactly opposite behaviour is in the declining phase. It is also clear that four basic spectral states form a hysteresis loop during the outburst, in that the way the accretion rates change in the rising phase is different from that in the declining phase.
(i) Hard State in Rising phase:

RXTE PCA started monitoring the source nine days after reported X-ray flaring activity (Tomsick 2010) observed with MAXI/GSC onboard ISS on 2010 January 03 (Yamaoka et al. 2010). From the first observation day (2010 January 12; MJD = 55208), the source was in hard state with increasing contribution to
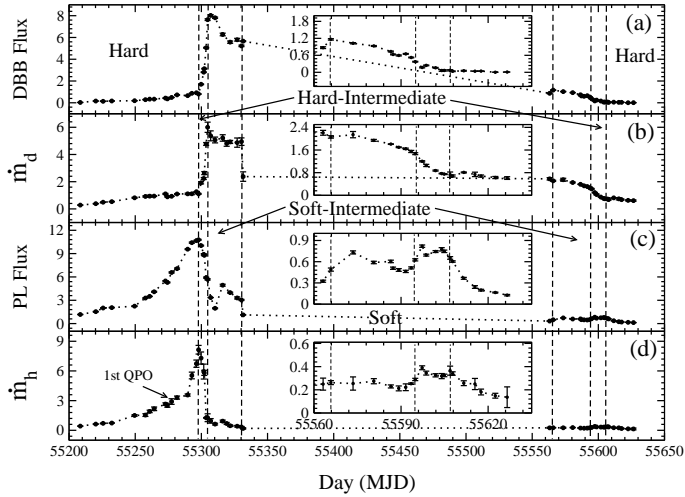
Figure 3. In top panel (a), the variation of combined disk black body (DBB) and power-law (PL) model fitted DBB spectral flux and in panel (c), the variation of PL spectral flux (both in units of 10^{-9} $ergs$ cm^{-2} s^{-1}) in $2.5 - 25$ keV energy range are shown. In panel (b), the variation of TCAF model fitted Keplerian disk rate $\dot{m}_d$ and in bottom panel (d), the variation of sub-Keplerian halo rate $\dot{m}_h$ (both in $\dot{M}_{Edd}$) in the same energy band are shown.
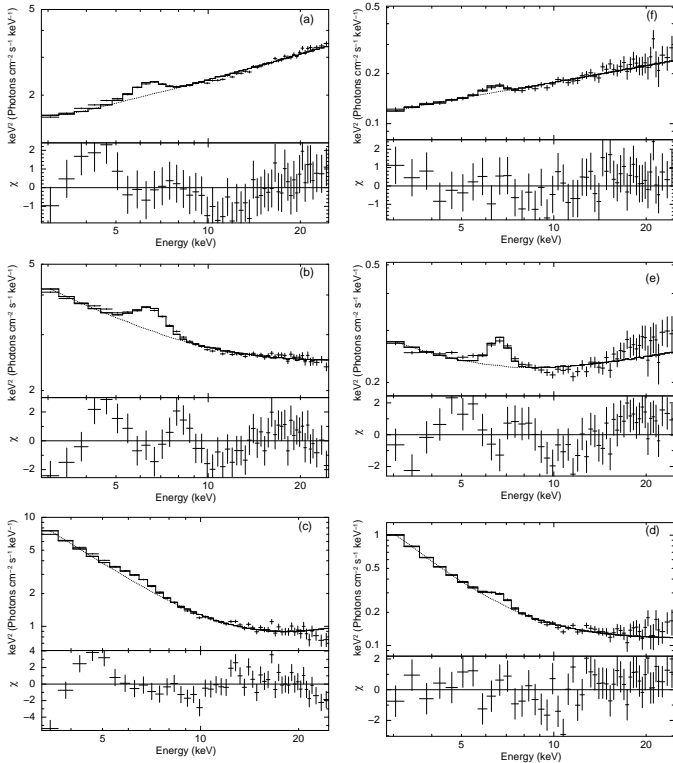
Figure 4. TCAF model fitted $2.5 - 25$ keV PCA spectral flux, $E^2 f(E)$ in units of keV^2 ($Photons$ cm^{-2} s^{-1} keV^{-1}) with variation of $\Delta\chi$, selected from the six different spectral states whose results are marked with (a-f), presented in Table Appendix I. Left panel spectra are from rising phase and right panel spectra are from declining phase of the outburst. From top to bottom, hard, hard-intermediate and soft-intermediate states spectra are shown.

total flux as well as percentage of non-thermal PL or sub-Keplerian halo rate (see, Figs. 1 & 3). The source was observed in this spectral state till 2010 April 10 (MJD = 55296.49). In this so-called hard state the flow is dominated by halo rates. QPOs are not observed for initial ~ 68 days up to 2010 March 19 (MJD = 55274.35), which is quite unusual in transient black hole candidates (Debnath et al. 2008, 2013, see,). ARR increases monotonically and reached its maximum value (~ 7.38) during rising phase (as well as the entire outburst) on 2010 April 11 (MJD = 55297.89), where we observe (Paper II) a transition from hard to hard-intermediate spectral state. ARR being maximum, the contribution from a Comptonized hot sub-Keplerian flow rate reached its maximum value with respect to thermally cool Keplerian flow rate. From Fig. 2, it is clear that during this phase of the outburst, the shock location (X_s) as well as shock height (h_{shk}) initially decrease with time (day) and then settle down to roughly a constant value. The shock is found to be weaker as the day progresses, initially slowly and then rapidly (see, Fig. 2b). Shock temperature (T_{shk}) initially increases, then settles down to a constant value, before decreasing rapidly, starting from the day when the first QPO is observed. While the shock location is generally decreasing, in the rising phase, it was not seen to be strictly monotonic as assumed to be the case in Debnath et al. (2010). This may be because (a) the flow in CENBOL is not streamlined. Turbulence can cause shock movements a bit erratic. (b) Assumption of a constant accretion rate throughout the disk may not be correct in a rapidly evolving system. This may have forced the fitted shock location not to maintain monotonicity and (c) Comptonization was assumed only due to the CENBOL region. Neglecting any contribution from jets could easily change the fitted parameters either way. These causes affect the compression ratio of the shock. The shock location and compression ratio together decide the infall time scale in the post-shock region which in turn decides the QPO frequency.

(ii) Hard-Intermediate State in the Rising phase :

Source was in this state for next ~ 6 days after transition day (MJD = 55297.89). During this phase, QPO frequency is observed to increase monotonically as before from spectral transition day (MJD = 55297.89; where 1.241 Hz QPO is observed) to 2010 April 17 (MJD = 55303.61; where maximum value of QPO frequency of 5.692 Hz is observed). On the next day, on 2010 April 18 (MJD = 55304.72), observed QPO frequency (5.739 Hz) remained very similar and after that QPO appeared sporadically. This happens to be the day when the transition to the soft-intermediate state took place (Paper II). On this day, ARR reaches its lowest value compared to what it had for preceding more than three weeks. It is to be noted that during this spectral state, as the day progressed, supply of thermally cool Keplerian matter ($\dot{m}_d$) is increased, at the same time supply of sub-Keplerian flow ($\dot{m}_h$) is decreased. As a result of that, ARR is decreased monotonically. The overall spectra are still dominated by hard radiation from high halo rates (see, Figs. 1-3).

(iii) Soft-Intermediate State in the Rising phase:

Source was observed in this spectral state for the next ~ 26 days from spectral transition day (2010 April 18; MJD = 55304.72), where sporadic QPOs of frequencies ~ 4.7 − 6.6 Hz are observed. During this spectral state, PCA count rates as well as total spectral flux/accretion rates are initially increased and then decreased (Paper II). This is because of initial increase in PL flux/sub-Keplerian rates and decrease in DBB flux/Keplerian rate. As a result, ARR varies within a short range ~ 0.07−0.21. In this state, the last prominent QPO of 4.687 Hz is observed on 2010 May 14 (MJD = 55330.29). On the next day, 2010 May 15 (MJD = 55331.55) no QPO is observed, where both disk and halo rates are decreased suddenly from its previously observed values. During this spectral

state, flickering behaviors of shock temperature and compression ratio are observed (see, Fig. 2). As the disk rate rises, spectral index becomes very sensitive to the disk and halo parameters (CT95). It is possible that flickering of the fitted parameters is because of that.

(iv) Soft State:

Present version of fits file is not suitable to fit spectra from this spectral state as the flow essentially contains a single standard Keplerian disk component with a weak power-law component due to bulk motion Comptonization (which has not been included in this version of TCAF fits model) and non-thermal component (Zdziarski et al. 2001; Chakrabarti & Mandal 2006). Still, we fitted three spectra including two spectral transition days with acceptable values of reduced χ^2 (< 3). The source stayed in this spectral state for a long period of time ($\sim$ 8 months). On soft to soft-intermediate transition day, 2011 January 04 (MJD = 55565.83) ARR is observed to be $\sim$ 0.13.

(v) Soft-Intermediate State in Declining phase:

The source was observed in this spectral state for about a month, where some variation in ARR ($0.13 - 0.16$) is observed, because of the reductions of $\dot{m}_d$ and $\dot{m}_h$ (see, Figs. 1-3). During this phase, similar to rising soft-intermediate spectral state, QPOs are observed to be sporadic (at $\sim$ $0.7 - 2$ Hz). On 2011 February 02 (MJD = 55594.90), another spectral transition from soft-intermediate to hard-intermediate state is observed, due to rise in $\dot{m}_h$ and decrease in $\dot{m}_d$, where a prominent QPO of frequency 6.420 Hz is observed.

(vi) Hard-Intermediate State in Declining phase:

Source was observed in this spectral state for the next $\sim$ 10 days starting from spectral transition (soft-intermediate to hard-intermediate) day (2011 February 02; MJD = 55594.90). During this phase, similar to declining hard-intermediate state of other transient BHCs (e.g., Debnath et al. 2008 for 2005 outburst of GRO J1655-40; Debnath et al. 2013 for 2010 & 2011 outbursts of H 1743-322) QPO frequencies are observed to decrease monotonically. As time passed, ARR increased monotonically due to daily rise in $\dot{m}_h$ rate and fall in $\dot{m}_d$ rate. ARR reaches its maximum value for the declining phase ($\sim$ 0.50) on 2011 February 14 (MJD = 55606.90), where QPO of frequency 0.175 Hz is observed. During this phase of the outburst, a slow increase in shock strength, shock height and temperature are observed. Shock also moved outward (see, Fig. 2).

(vii) Hard State in Declining phase:

The source was observed in this spectral state till the end of observational data set (2011 March 06; MJD = 55626.56). In this phase, prominent QPOs are observed only for two days, where QPO frequency is decreased from 0.175 Hz to 0.136 Hz. As the day progresses, both types of accretion rates ($\dot{m}_d$ and $\dot{m}_h$) decrease due to less supply of fresh matter (reduced viscosity). Thus ARR decreases monotonically and reaches a value of ($\sim$ 0.22) on the last day of the observation (MJD = 55626.56). During this state, a decrease in shock temperature with rapid rise in shock strength and height was seen. Also, shock is found to accelerate away from the black hole (see, Fig. 2).

5 DISCUSSION AND CONCLUDING REMARKS

For the first time, spectral properties of GX 339-4 during its recent 2010-11 outburst have been studied in detail and the spectra were fitted using two component advective flow (TCAF) model after its inclusion as an additive table model in HEASARC's spectral analysis software package XSPEC. For the inclusion of the model in XSPEC, a *fits* file was generated with $\sim$ 4×10^5 model spectra created by varying input parameters in the CT95 code, modified to include general shock location and shock strengths. For data analysis, we use RXTE/PCA spectral data in $2.5 - 25$ keV energy band. We analyzed a total of 50 observations spread over the entire outburst with TCAF model and compare our results with a combined DBB and PL model fitted results (Paper II). Variation of two component (Keplerian and sub-Keplerian) accretion rates extracted from TCAF model spectral fits are found to be consistent with DBB and PL model fluxes (see, Figs. 1 & 3). The results are summarized in Table 'Appendix I'. What we found is that the ratio of sub-Keplerian halo rate and standard Keplerian disk rate, namely ARR, may play a very important role in deciding state transitions. For instance ARR was found to have a local sharp maximum, both in the rising and the declining phases, on the day of transition between the hard state and the hard-intermediate state. Hard and hard-intermediate states are dominated by the halo rate, whereas the other two states are dominated by the disk rate. Hard and intermediate (hard-intermediate, and soft-intermediate) spectra fit extremely well with our current TCAF *fits* file, since in these states, two components are prominent. Soft state is dominated by the standard Keplerian disk alone and better fits are achieved when $\dot{m}_h \rightarrow 0$. In future, the fits file will be expanded with finer grids for this regime. The fact that the present version of TCAF fits deteriorate in soft states is a direct indication of the absence of shocks in this state. Recently, Mondal & Chakrabarti (2013), self-consistently solved transonic flow problem with Compton cooling. We hope to incorporate this into our code in future.

After fitting with TCAF, a clearer physical picture of what happens in an outburst emerges. Two types of accretion rates are found to vary independently. At the beginning of the outburst, spectra are dominated by low angular-momentum, thermally hot sub-Keplerian flow ($\dot{m}_h$) and the object is in a hard/low-hard state. As the outburst progresses, accretion rate of the Keplerian component ($\dot{m}_d$) increases and the object enters into a soft spectral state via two intermediate (hard-intermediate and soft-intermediate) spectral states. During the declining phase of the outburst, Keplerian disk recedes while the sub-Keplerian rate remains roughly the same or increases slightly, which makes the spectrum harder. So, at the end phase of the outburst, the source moves again in the hard state via two intermediate (soft-intermediate and hard-intermediate) spectral states. During this outburst of GX 339-4, maximum values of $\dot{m}_h$ (=8.14) and $\dot{m}_d$ (=5.99) are observed on 2010 April 11 (MJD = 55297.88) and 2010 April 18 (MJD = 55304.72) respectively. Since the sub-Keplerian matter moves roughly in a free-fall time scale, while the Keplerian disk moves in a viscous time scale, this lag is expected. This delay may provide an estimate of viscosity in the Keplerian component. This will be dealt with elsewhere.

Evolution patterns of the location of the shock (X_s in r_g unit) and height of the shock (h_{shk} in r_g unit) are more or less similar during this outburst of GX 339-4. During the rising phase of the outburst, as the day progresses, these two values generally decrease with time (day) and during the declining phase of the outburst, opposite scenario is observed. During rising phases of the outburst, the shock compression ratio (R) decreased initially slowly and then rapidly before it settled down to a lower value ($\sim$ 1.05). During the declining phase, it increased almost monotonically. In the same way, CENBOL surface temperature (T_{shk} in 10^{10} K) initially increased rapidly, then remained more or less constant at $\sim$ $4 - 5$. Interestingly, after the first observed QPO day (MJD = 55277), it rapidly decreased until the transition day of hard to hard-intermediate state. During declining hard state, T_{shk}

is observed to decrease monotonically, whereas during intermediate states T_{shk} is found to be non-monotonic. In the present TCAF *fits* file, shock locations, shock strengths (inverse of the compression ratio), shock heights, and shock temperatures are all calculated simultaneously without taking care of outflows, if any. It is to be noted that in the present version of TCAF fits file, the input parameters shock location and compression ratio both could be calculated from the fundamental flow equations, namely, from a set of energy and angular momentum of the accretion flow (C90a Mondal, Chakrabarti & Debnath 2014b). In that case, our fit would yield more fundamental parameters. This will be done in next version of the TCAF model *fits* file. Variation of angular momentum would also give a measure of viscosity. The general trend of the shock location is on an average the same as in Paper II. There is, however, some discrepancy, because in Paper II, no spectral data was used to compute shock locations. Rather, an approximate algebraic relation between shock location and QPO frequency was used and that yielded quite high values of shock locations. The compression ratio was adjusted suitably to fit the QPO frequency variation. In the present case, shock locations and compression ratios are obtained by TCAF fits and therefore are more realistic. We find that there are some fluctuations in shock locations on the top of monotonic behaviour. Part of the reason could be that along with Compton cooling which pushes the shock towards the black hole, presence and absence of winds (which is not considered here), which reduces density in CENBOL also affects the shock location. Another important assumption was that the accretion rate was treated as a constant throughout the disk (Dutta & Chakrabarti 2010), which is questionable in an evolving system. However, the general tendency of shock location remained acceptable and the behaviour is found to be consistent with anticipated behaviour. Another source of fluctuation could be that as the accretion rate goes up, the CENBOL switches from becoming an ion pressure supported to a radiation pressure supported. So the size of the CENBOL could grow at very soft state. In future, we will try to incorporate these aspects in our modified TCAF model *fits* file.

Almost all the spectra are fitted with an Iron line of $\sim 6.2 - 6.7$ keV (by adding a Gaussian model component along with TCAF model), except those where *LW* (line width in keV) and *LD* (line depth) are absent in Table I of Appendix. The non-Gaussian model fitted spectra are seen only in extreme two ends (hard states) of the outburst. Given that the resolution of RXTE/PCA is not good for line studies, a general nature of the Iron line evolution is observed. We do see a progressive widening of Iron line as we go from hard states to softer states. Similar variation is also observed for line depth. According to TCAF, lines are formed in the Keplerian disk just outside CENBOL and thus the solid angle to produce line widths would be large enough ($\sim 2\pi$). Also as the state becomes softer, rotational velocity increases as CENBOL moves in. This increases line broadening. Thermal broadening also increases, as the disk temperature rises. In future, we will include Iron line to generate *fits* file, since its width would be related to shock properties.

Most natural assumption of the cause of an outburst, i.e., rise in flow rates, is possibly a rise in activity of the companion together with a rise in viscosity, perhaps of magnetic origin, owing to enhanced magnetic activity in the companion, or convective turbulence at the outer disk. If we assume that it is the sub-Keplerian component rate that is easy to change by the companion, the interpretations become easier. During the rising phase of an outburst, viscosity causes an increase in the accretion rate of Keplerian component since angular momentum of a sub-Keplerian flow could

be easily re-distributed to produce a Keplerian disk (Chakrabarti & Molteni, 1995; Giri & Chakrabarti, 2013). Thus, a soft state is achieved in viscous time scale. As long as high (super-critical, C90ab) viscosity persists, the object stays in the soft state. When viscosity is reduced to sub-critical value, declining phase starts with a reduction of the Keplerian rate. Keplerian disk itself is retracted due to lack of conversion. A simple estimate of viscosity parameter suggests that α should increase from 0.001 to 0.02 from the first day to the day it came to the soft state (Mondal, Chakrabarti & Debnath 2015). These α values are consistent with what simulations with MRI indicate (Arlt & Rdiger 2001; Masada & Sano 2009). In the literature, a few models require higher viscosity to explain the origin of QPOs and spectral states (Mauche 2002; Titarchuk & Fiorito 2004). This could be because their disk is Keplerian with high angular momentum, which requires high viscosity ($\sim 0.1 - 0.5$) to transport angular momentum. On the contrary, TCAF assumes a sub-Keplerian with low angular momentum, where lesser amount of viscosity is sufficient to explain the spectral states and origin of QPO frequencies (Mondal, Chakrabarti & Debnath 2015) through shock formation and its oscillation.

Generally type 'C' QPOs are observed in hard, and hard-intermediate spectral states and type 'B' QPOs are observed in soft-intermediate spectral states (see, van der Klis 2004). During hard and hard-intermediate spectral states, QPOs are observed continuously starting from the day when sudden rise in ARR is observed (see, Figs. 1 & 3). It has been noticed that ARR reached its maximum values on the day the transition between hard to hard-intermediate states takes place. During soft-intermediate states, QPOs are observed sporadically as this state is slightly dominated by thermally cooler Keplerian flows, and QPOs are seen when sub-Keplerian halo rate rises (see, Figs. 1 & 3). This perception is more prominent in the rising soft-intermediate state because during the declining phase, total accretion rate is decreased as a whole. No LFQPOs are observed in soft states because oscillatory shock conditions which are required for the generation of QPOs are not satisfied in a 'sub-sonic' Keplerian disk, which after all, dominates this state. As a result, accretion disk becomes thermally cool approximately at a constant temperature (see, Fig. 7a of Paper II). It appears that there is an association of a (though, sometimes weak) *peak* of ARR with a state transition. ARR has a local maximum on the day of transition between hard and hard-intermediate states. This important finding was possible only after fitting with the TCAF solution. Of course, TCAF solution depends strongly on the behaviour of the companion. Unless the process of matter supply is well understood, predictability of the subject is limited to a duration much less than the stellar variability timescale.

According to the shock oscillation model by Chakrabarti and his collaborators in mid-90s, LFQPOs are originated due to oscillation of post-shock region (Molteni, Sponholz & Chakrabarti 1996; Chakrabarti, Acharyya & Molteni 2004) when resonance occurs between infall time scale and cooling time scale in CENBOL or when Rankine-Hugoniot conditions are not satisfied to form a steady shock (Ryu, Chakrabarti, & Molteni 1997). So, one can obtain the QPO frequency if one knows instantaneous shock location and compression ratio (assuming turbulence, which can increase infall time, is absent). Since we directly extract shock parameters from TCAF model fits, we should be able to predict frequency of low frequency QPOs, if present, and make a comparative study with POS model (Chakrabarti et al. 2005, 2008, 2009; Debnath et al. 2010, 2013; Nandi et al. 2012) fitted results. Indeed, we find that while going from hard-intermediate to soft-intermediate states, the rms value of QPOs is suddenly reduced (see, Table A.2 of Paper

II). This points to the fact that the oscillating body (here the shock) is getting more and more diffused. Our finding of weakening of the shock strength corroborates with the general conclusion drawn from rms values. Indeed, weaker shocks could just be density enhancements due to centrifugal barrier and thus would produce 'B' type QPOs. This aspect will be looked into in a future work.

REFERENCES

Allured, R., Tomsick, J. A., Kaaret, P. & Yamaoka, K., 2013, ApJ, 774, 135

Arlt, R. & Rdiger, G., 2001, A & A, 374, 1035

Belloni, T., Homan, J., Casella, P., et al., 2005, A&A, 440, 207

Buxton, M. M., Bailyn, C. D., & Capelo, H. L., et al., 2012, AJ, 143, 130

Cadolle, B. M. et al., 2012, A & A, 544, 2

Chakrabarti, S. K., 1989, MNRAS, 340, 7 (C89)

Chakrabarti, S. K., 1990a, "Theory of Transonic Astrophysical Flows", World Scientific (Singapore) (C90a)

Chakrabarti, S. K., 1990b, ApJ, 362, 406 (C90b)

Chakrabarti, S. K. & Molteni, D., 1995, MNRAS, 272, 80 (CM95)

Chakrabarti, S. K. & Titarchuk, L. G., 1995, ApJ, 455, 623 (CT95)

Chakrabarti, S. K., 1996, ApJ, 464, 664

Chakrabarti, S. K., 1997, ApJ, 484, 313 (C97)

Chakrabarti, S.K., 1999, A & A, 351, 185

Chakrabarti, S. K., Acharyya, K., & Molteni, D., 2004, A&A, 421, 1

Chakrabarti, S. K., Nandi, A., & Debnath, D., et al., 2005, IJP 79(8), 841 (astro-ph/0508024)

Chakrabarti, S. K. & Mandal, S. 2006, ApJ, 642, L49

Chakrabarti, S. K., Debnath, D., & Nandi, A., et al., 2008, A&A, 489, L41

Chakrabarti, S. K., Dutta, B. G. & Pal, P. S., 2009, MNRAS, 394, 1463

Corbel, S., Coriat, M., & Brocksopp, C., et al., 2013a, MNRAS, 428, 2500

Corbel, S., Aussel, H., Broderick, J. W., et al., 2013b, MNRAS, 431, 107

Debnath, D., Chakrabarti, S. K., Nandi, A., et al., 2008, BASI, 36, 151

Debnath, D., Chakrabarti, S. K., & Nandi, A., 2010, A&A, 520, 98 (Paper I)

Debnath, D., Chakrabarti, S. K., & Nandi, A., 2013, AdSpR, 52, 2143

Debnath, D., Chakrabarti, S. K., & Mondal, S., 2014, MNRAS, 440, L121 (DCM14)

Dincer, T., Kalemci, E., & Buxton, M. M., et al., 2012, ApJ, 753, 55

Dutta, B. G., & Chakrabarti, S. K., 2010, MNRAS, 404, 2136

Ebisawa, K., Titarchuk, L., & Chakrabarti, S. K., 1996, PASJ, 48, 59

Giri, K., & Chakrabarti, S. K., 2013, MNRAS, 430, 2836

Giri, K., & Chakrabarti, S. K., 2014, MNRAS (submitted)

Haardt, F., & Maraschi, L., 1993, ApJ, 413, 507

Homan, J. & Belloni, T., 2005, Ap&SS, 300, 107

Hua, X. & Titarchuk, L.G. 1995, ApJ, 449, 188

Hynes, R. I., Steeghs, D., & Casares, J., et al., 2003, ApJ, 583, L95

Hynes, R. I., Steeghs, D., & Casares, J., et al., 2004, ApJ, 609, 317

Landau, L. D. & Lifshitz, E. M., 1959, "Fluid Mechanics", Oxford

Maccarone, T. J. & Coppi, P. S., 2003, MNRAS, 338, 189

Mandal, S. & Chakrabarti, S. K., 2010, ApJ, 710, L147

Markert, T. H., Canizares, C. R., & Clark, G. W., et al., 1973, ApJ, 184, L67

Masada, Y. & Sano, T. 2009, IAU Symposium No. 259, 121

Mauche, C., 2002, ApJ, 580, 423

McClintock, J. E., & Remillard, R. A., 2006, in Compact Stellar X-ray Sources, Cambridge, Astrophysical Ser., vol. 39, ed. W. Lewin & M. van der Klis (Cambridge Univ. Press), 157

Mondal, S., & Chakrabarti, S. K., 2013, MNRAS, 431, 2716

Mondal, S., Debnath, D., & Chakrabarti, S. K., 2014a, ApJ, 786, 4 (MDC14)

Mondal, S., Chakrabarti, S. K., & Debnath, D., 2014b, Ap&SS, 353, 223

Mondal, S., Chakrabarti, S. K., & Debnath, D., 2015, ApJ, 798, 57

Molteni, D., Lanzafame, G. & Chakrabarti, S.K., 1994, ApJ, 425, 161

Molteni, D., Sponholz, H. & Chakrabarti, S. K., 1996, ApJ, 457, 805

Motta, S., Belloni, T., & Homan, J., 2009, MNRAS, 400, 1603

Motta, S., Munoz-Darias, T., & Casella, P., et al., 2011, MNRAS, 418, 2292

Nandi, A., Debnath, D., & Mandal, S., et al., 2012, A&A, 542, 56 (Paper II)

Nowak, M. A., Wilms, J., & Dove, J. B., 1999, ApJ, 517, 355

Okuda, T., Teresi, V. & Molteni, D., 2007, MNRAS 377, 1431

Paczyński, B., & Witta, P. J., 1980, A&A, 88, 23

Paczyński, B., & Bisnovatyi-Kogan, G., 1981, Acta Astron., 31, 283

Rahoui, F., Coriat, M., & Corbel, S., et al., 2012, MNRAS, 422, 2202

Remillard, R. A., & McClintock, J. E., 2006, ARA&A, 44, 49

Ryu, D., Chakrabarti, S. K. & Molteni, D., 1997, ApJ, 474, 378

Shakura, N. I., & Sunyaev, R. A., 1973, A&A, 24, 337 (SS73)

Shidatsu, M., Ueda, Y., Tazaki, F., et al., 2011, PASJ, 63, 785

Shidatsu, M., Ueda, Y., Nakahira, S., et al., PASJ, 63, 803

Shimura, T., & Takahara, F., 1995, ApJ, 445, 780

Singh, C. B., & Chakrabarti, S. K., 2011, MNRAS, 410, 2414

Sobolev, V.V. 1975, Light Scattering in Planetary Atmosphere (Oxford: Pergamon)

Stiele, H., Motta, S., & Muñoz-Darias, T., et al., 2011, MNRAS, 418, 1746

Sunyaev, R.A., & Titarchuk, L. G., 1980, ApJ, 86, 121

Sunyaev, R.A., & Titarchuk, L. G., 1985, A&A, 143, 374

Tomsick, J. A., 2010, ATel, 2384, 1

Titarchuk, L & Fiorito, R., 2004, ApJ, 612, 988

Titarchuk, L.G., & Seina, E. 2009, ApJ, 706, 1463

Titarchuk, L.G., & Zannias, T. 1998, ApJ, 493, 863

van der Klis, M., 2004, AN, 326, 798

Yamaoka, K., Nakahira, S., & Mihara, T., et al., 2010, ATel, 2380, 1

Yan, Z. & Yu, W., 2012, MNRAS, 427, L11

Zdziarski, A. A., Grove, J. E., Poutanen, J., Rao, A. R., & Vadawale, S. V., 2001, ApJ, 554, L45

Zdziarski, A. A., Lubinski, P., & Gilfanov, M., et al., 2003, MNRAS, 342, 355

Appendix I

2.5-25 keV TCAF Model Fitted Parameters With QPOs

Obs	Id	MJD	$\dot{m}_d$ ($\dot{M}_{Edd}$)	$\dot{m}_h$ ($\dot{M}_{Edd}$)	ARR	X_s (r_g)	R	h_{shk} (r_g)	T_{shk} ($10^{10}K$)	R_z (km)	$LW^{\dagger}$ (keV)	$LD^{\dagger}$	$QPO^{\dagger\dagger}$ (Hz)	χ^2/DOF
(1)	(2)	(3)	(4)	(5)	(6)	(7)	(8)	(9)	(10)	(11)	(12)	(13)	(14)	(15)
1	X-01-00	55208.49	$0.281^{\pm0.010}$	$0.422^{\pm0.011}$	$1.508^{\pm0.093}$	$148.0^{\pm2.106}$	$1.670^{\pm0.011}$	$93.65^{\pm1.950}$	$0.885^{\pm0.012}$	$1.837^{\pm0.147}$	–	–	–	40.99/42
2	X-03-00	55220.18	$0.382^{\pm0.013}$	$0.630^{\pm0.012}$	$1.649^{\pm0.088}$	$77.94^{\pm2.077}$	$1.629^{\pm0.018}$	$48.99^{\pm1.847}$	$1.668^{\pm0.041}$	$2.321^{\pm0.118}$	–	–	–	72.31/45
3	X-04-00	55225.72	$0.493^{\pm0.014}$	$0.707^{\pm0.011}$	$1.434^{\pm0.063}$	$49.51^{\pm0.586}$	$1.644^{\pm0.029}$	$31.20^{\pm0.920}$	$2.659^{\pm0.063}$	$2.339^{\pm0.106}$	0.31	1.09e-3	–	76.46/43
4	X-05-00	55232.27	$0.531^{\pm0.017}$	$0.732^{\pm0.018}$	$1.379^{\pm0.078}$	$32.31^{\pm0.463}$	$1.650^{\pm0.034}$	$20.38^{\pm0.712}$	$4.128^{\pm0.115}$	$2.093^{\pm0.108}$	0.44	1.79e-3	–	51.11/42
5	X-07-00	55249.53	$0.817^{\pm0.036}$	$1.503^{\pm0.083}$	$1.839^{\pm0.183}$	$33.20^{\pm0.737}$	$1.635^{\pm0.021}$	$20.89^{\pm0.732}$	$3.993^{\pm0.096}$	$1.941^{\pm0.108}$	0.52	2.01e-3	–	65.43/42
6	X-08-00	55257.71	$0.915^{\pm0.044}$	$1.542^{\pm0.139}$	$1.685^{\pm0.233}$	$24.32^{\pm1.081}$	$1.549^{\pm0.043}$	$15.02^{\pm1.085}$	$5.311^{\pm0.266}$	$1.779^{\pm0.119}$	0.56	3.72e-3	–	41.86/42
7	X-09-00	55260.92	$0.937^{\pm0.073}$	$1.910^{\pm0.126}$	$2.038^{\pm0.293}$	$23.71^{\pm0.263}$	$1.354^{\pm0.027}$	$13.45^{\pm0.417}$	$4.602^{\pm0.117}$	$1.775^{\pm0.110}$	0.53	4.59e-3	–	44.17/43
8	X-09-02	55264.26	$0.940^{\pm0.019}$	$2.174^{\pm0.182}$	$2.313^{\pm0.240}$	$21.43^{\pm0.848}$	$1.313^{\pm0.013}$	$11.79^{\pm0.583}$	$4.810^{\pm0.143}$	$1.775^{\pm0.127}$	0.58	3.73e-3	–	48.48/43
9	X-10-05	55272.82	$1.102^{\pm0.037}$	$2.650^{\pm0.126}$	$2.405^{\pm0.195}$	$18.78^{\pm1.047}$	$1.270^{\pm0.012}$	$9.920^{\pm0.647}$	$5.096^{\pm0.190}$	$2.192^{\pm0.129}$	0.62	7.28e-3	–	51.70/44
10	X-11-00	55274.33	$0.888^{\pm0.026}$	$2.500^{\pm0.174}$	$2.815^{\pm0.278}$	$21.58^{\pm0.869}$	$1.292^{\pm0.020}$	$11.65^{\pm0.650}$	$4.601^{\pm0.164}$	$2.041^{\pm0.200}$	0.61	6.27e-3	–	39.92/43
11	X-11-02	55277.47	$0.928^{\pm0.011}$	$2.907^{\pm0.283}$	$3.133^{\pm0.342}$	$20.92^{\pm1.040}$	$1.321^{\pm0.017}$	$11.58^{\pm0.725}$	$4.999^{\pm0.189}$	$2.378^{\pm0.154}$	0.65	1.08e-2	0.102	43.55/43
12^a	X-12-00	55281.59	$1.096^{\pm0.015}$	$3.303^{\pm0.157}$	$3.014^{\pm0.184}$	$22.35^{\pm0.497}$	$1.302^{\pm0.017}$	$12.18^{\pm0.430}$	$4.517^{\pm0.109}$	$3.088^{\pm0.123}$	0.69	1.34e-2	0.134	46.72/43
13	X-13-00	55289.62	$1.107^{\pm0.050}$	$3.566^{\pm0.110}$	$3.221^{\pm0.245}$	$23.11^{\pm0.309}$	$1.106^{\pm0.033}$	$8.783^{\pm0.380}$	$2.122^{\pm0.077}$	$3.519^{\pm0.151}$	0.67	1.82e-2	0.261	72.14/43
14	X-13-05	55292.78	$1.110^{\pm0.066}$	$5.542^{\pm0.339}$	$4.993^{\pm0.602}$	$22.36^{\pm0.692}$	$1.055^{\pm0.029}$	$6.417^{\pm0.375}$	$1.252^{\pm0.054}$	$4.735^{\pm0.135}$	0.70	3.22e-2	0.363	72.43/43
15	X-14-01	55296.25	$1.262^{\pm0.013}$	$6.734^{\pm0.367}$	$5.336^{\pm0.346}$	$32.30^{\pm0.513}$	$1.068^{\pm0.042}$	$10.18^{\pm0.562}$	$1.031^{\pm0.049}$	$6.665^{\pm0.204}$	0.71	1.89e-2	1.026	64.21/43
16	X-14-02	55297.88	$1.103^{\pm0.035}$	$8.143^{\pm0.438}$	$7.383^{\pm0.631}$	$19.28^{\pm0.125}$	$1.063^{\pm0.026}$	$5.877^{\pm0.182}$	$1.651^{\pm0.046}$	$5.454^{\pm0.185}$	0.77	2.11e-2	1.241	80.36/43
17^b	X-14-06	55299.77	$1.921^{\pm0.084}$	$7.302^{\pm0.613}$	$3.801^{\pm0.485}$	$25.71^{\pm0.781}$	$1.171^{\pm0.015}$	$11.72^{\pm0.506}$	$2.732^{\pm0.076}$	$6.098^{\pm0.123}$	0.75	2.65e-2	2.420	71.49/43
18	X-14-05	55301.79	$2.234^{\pm0.074}$	$5.936^{\pm0.754}$	$2.657^{\pm0.426}$	$29.69^{\pm0.662}$	$1.177^{\pm0.014}$	$13.70^{\pm0.469}$	$2.411^{\pm0.056}$	$11.62^{\pm0.122}$	0.76	3.28e-2	3.643	68.98/43
19	X-15-00	55302.20	$2.632^{\pm0.111}$	$5.810^{\pm0.258}$	$2.207^{\pm0.191}$	$23.64^{\pm0.030}$	$1.186^{\pm0.018}$	$11.09^{\pm0.182}$	$3.162^{\pm0.050}$	$8.603^{\pm0.105}$	0.74	2.81e-2	4.177	70.68/43
20	X-15-01	55303.61	$4.772^{\pm0.103}$	$1.259^{\pm0.036}$	$0.264^{\pm0.013}$	$46.40^{\pm0.310}$	$1.101^{\pm0.037}$	$17.29^{\pm0.697}$	$0.993^{\pm0.037}$	$12.26^{\pm0.164}$	0.68	1.98e-2	5.692	76.33/43
21	X-15-02	55304.72	$5.999^{\pm0.377}$	$1.271^{\pm0.398}$	$0.212^{\pm0.080}$	$51.86^{\pm5.454}$	$1.073^{\pm0.054}$	$16.86^{\pm2.621}$	$0.675^{\pm0.069}$	$16.39^{\pm0.159}$	0.71	2.56e-2	5.739	112.7/43
22	X-15-05	55307.03	$5.371^{\pm0.366}$	$0.955^{\pm0.230}$	$0.178^{\pm0.055}$	$52.92^{\pm6.125}$	$1.085^{\pm0.074}$	$18.36^{\pm3.377}$	$0.753^{\pm0.095}$	$21.83^{\pm0.122}$	0.78	1.03e-2	–	105.3/43
23	X-16-01	55310.34	$5.066^{\pm0.214}$	$0.628^{\pm0.088}$	$0.124^{\pm0.023}$	$65.84^{\pm7.246}$	$1.079^{\pm0.039}$	$22.14^{\pm3.237}$	$0.567^{\pm0.052}$	$53.70^{\pm0.119}$	0.80	9.11e-3	–	121.6/42
24^c	X-17-00	55316.12	$5.214^{\pm0.237}$	$0.924^{\pm0.104}$	$0.177^{\pm0.028}$	$52.59^{\pm6.788}$	$1.086^{\pm0.051}$	$18.33^{\pm3.227}$	$0.765^{\pm0.085}$	$21.02^{\pm0.139}$	0.83	2.01e-2	6.074	100.4/43
25	X-17-03	55319.13	$4.808^{\pm0.203}$	$0.690^{\pm0.101}$	$0.144^{\pm0.027}$	$48.56^{\pm5.958}$	$1.067^{\pm0.049}$	$15.21^{\pm2.564}$	$0.670^{\pm0.072}$	$23.16^{\pm0.145}$	0.82	2.18e-2	–	95.43/43
26	X-17-05	55321.73	$4.922^{\pm0.110}$	$0.463^{\pm0.087}$	$0.094^{\pm0.020}$	$38.00^{\pm9.964}$	$1.170^{\pm0.044}$	$17.29^{\pm5.183}$	$1.817^{\pm0.306}$	$16.56^{\pm0.158}$	0.75	1.90e-2	5.250	102.8/43
27	X-18-04	55327.04	$4.871^{\pm0.341}$	$0.413^{\pm0.076}$	$0.085^{\pm0.022}$	$33.13^{\pm8.474}$	$1.126^{\pm0.041}$	$13.48^{\pm3.940}$	$1.674^{\pm0.275}$	$14.04^{\pm0.153}$	0.85	1.39e-2	4.776	92.36/42
28	X-19-00	55330.29	$4.945^{\pm0.275}$	$0.330^{\pm0.059}$	$0.067^{\pm0.016}$	$49.90^{\pm9.384}$	$1.196^{\pm0.051}$	$23.85^{\pm5.501}$	$1.517^{\pm0.207}$	$60.31^{\pm0.120}$	0.81	7.66e-3	4.687	98.30/42
29	X-19-01	55331.55	$2.375^{\pm0.347}$	$0.191^{\pm0.061}$	$0.080^{\pm0.037}$	$34.30^{\pm6.916}$	$1.127^{\pm0.064}$	$14.00^{\pm3.619}$	$1.625^{\pm0.256}$	$24.86^{\pm0.155}$	0.95	3.51e-3	–	95.24/43
30	Y-01-01	55563.14	$2.209^{\pm0.085}$	$0.249^{\pm0.052}$	$0.113^{\pm0.028}$	$31.06^{\pm10.42}$	$1.172^{\pm0.024}$	$14.19^{\pm5.051}$	$2.255^{\pm0.424}$	$17.16^{\pm0.210}$	0.53	2.01e-3	–	82.36/45
31	Y-01-02	55565.83	$2.062^{\pm0.043}$	$0.262^{\pm0.017}$	$0.127^{\pm0.011}$	$29.71^{\pm6.988}$	$1.064^{\pm0.041}$	$9.120^{\pm2.496}$	$1.066^{\pm0.166}$	$11.48^{\pm0.303}$	0.46	1.91e-3	–	54.05/42
32	Y-02-02	55573.47	$2.143^{\pm0.110}$	$0.254^{\pm0.057}$	$0.119^{\pm0.033}$	$29.75^{\pm1.639}$	$1.120^{\pm0.019}$	$11.88^{\pm0.856}$	$1.801^{\pm0.080}$	$13.63^{\pm0.143}$	0.48	2.77e-3	–	65.83/43
33	Y-03-02	55580.62	$1.941^{\pm0.034}$	$0.274^{\pm0.022}$	$0.141^{\pm0.014}$	$29.60^{\pm1.554}$	$1.055^{\pm0.025}$	$8.495^{\pm0.647}$	$0.935^{\pm0.047}$	$9.251^{\pm0.161}$	0.51	1.52e-3	–	53.78/43
34^d	Y-04-02	55586.50	$1.809^{\pm0.010}$	$0.229^{\pm0.013}$	$0.127^{\pm0.008}$	$32.74^{\pm0.476}$	$1.061^{\pm0.022}$	$9.839^{\pm0.347}$	$0.924^{\pm0.026}$	$12.62^{\pm0.145}$	0.45	1.54e-3	2.158	32.74/43
35	Y-05-00	55589.20	$1.697^{\pm0.014}$	$0.212^{\pm0.021}$	$0.125^{\pm0.013}$	$32.46^{\pm0.455}$	$1.061^{\pm0.027}$	$9.755^{\pm0.385}$	$0.932^{\pm0.030}$	$13.11^{\pm0.181}$	0.59	1.32e-3	–	38.45/42
36	Y-05-01	55591.62	$1.644^{\pm0.024}$	$0.222^{\pm0.029}$	$0.135^{\pm0.020}$	$29.59^{\pm0.174}$	$1.067^{\pm0.035}$	$9.267^{\pm0.358}$	$1.114^{\pm0.040}$	$10.74^{\pm0.183}$	0.63	1.70e-3	1.705	75.84/43
37	Y-05-02	55593.51	$1.549^{\pm0.037}$	$0.253^{\pm0.006}$	$0.163^{\pm0.008}$	$29.18^{\pm0.472}$	$1.055^{\pm0.022}$	$8.374^{\pm0.310}$	$0.949^{\pm0.027}$	$7.548^{\pm0.202}$	0.60	1.01e-3	1.742	61.58/43
38	Y-05-03	55594.90	$1.470^{\pm0.034}$	$0.289^{\pm0.010}$	$0.197^{\pm0.011}$	$23.34^{\pm0.368}$	$1.068^{\pm0.019}$	$7.357^{\pm0.247}$	$1.445^{\pm0.037}$	$2.668^{\pm0.172}$	0.58	1.89e-3	6.420	72.55/43
39	Y-06-00	55597.26	$1.201^{\pm0.020}$	$0.390^{\pm0.017}$	$0.325^{\pm0.020}$	$27.22^{\pm0.449}$	$1.055^{\pm0.012}$	$7.812^{\pm0.218}$	$1.020^{\pm0.020}$	$3.244^{\pm0.208}$	0.52	1.90e-3	4.684	59.78/43
40	Y-06-01	55598.67	$1.055^{\pm0.039}$	$0.344^{\pm0.017}$	$0.326^{\pm0.028}$	$29.78^{\pm0.354}$	$1.054^{\pm0.017}$	$8.476^{\pm0.237}$	$0.914^{\pm0.020}$	$5.334^{\pm0.104}$	0.43	1.88e-3	3.973	52.95/43
41^e	Y-06-02	55601.89	$0.873^{\pm0.019}$	$0.325^{\pm0.014}$	$0.372^{\pm0.024}$	$26.01^{\pm0.240}$	$1.092^{\pm0.014}$	$9.327^{\pm0.206}$	$1.670^{\pm0.029}$	$3.193^{\pm0.112}$	0.46	1.58e-3	1.322	70.01/43
42	Y-07-00	55603.99	$0.768^{\pm0.013}$	$0.318^{\pm0.022}$	$0.414^{\pm0.036}$	$37.53^{\pm1.007}$	$1.102^{\pm0.024}$	$14.04^{\pm0.683}$	$1.245^{\pm0.044}$	$2.825^{\pm0.133}$	0.42	6.47e-4	1.087	49.54/43
43	Y-07-03	55604.90	$0.749^{\pm0.013}$	$0.324^{\pm0.011}$	$0.433^{\pm0.022}$	$37.91^{\pm0.877}$	$1.111^{\pm0.035}$	$14.68^{\pm0.802}$	$1.319^{\pm0.057}$	$2.440^{\pm0.115}$	0.41	4.85e-4	1.149	44.19/43
44	Y-07-01	55606.90	$0.729^{\pm0.095}$	$0.365^{\pm0.039}$	$0.501^{\pm0.119}$	$30.49^{\pm0.387}$	$1.136^{\pm0.020}$	$12.78^{\pm0.387}$	$1.934^{\pm0.046}$	$1.676^{\pm0.108}$	0.32	4.42e-4	0.175	45.57/43
45^f	Y-07-02	55607.76	$0.684^{\pm0.036}$	$0.340^{\pm0.015}$	$0.497^{\pm0.048}$	$42.45^{\pm1.229}$	$1.181^{\pm0.018}$	$19.74^{\pm0.873}$	$1.695^{\pm0.050}$	$1.366^{\pm0.118}$	0.39	4.20e-4	0.136	47.24/43
46	Y-08-00	55611.61	$0.810^{\pm0.015}$	$0.257^{\pm0.021}$	$0.317^{\pm0.032}$	$49.67^{\pm4.026}$	$1.134^{\pm0.010}$	$20.69^{\pm1.860}$	$1.159^{\pm0.057}$	$1.971^{\pm0.138}$	0.20	1.44e-4	–	42.92/43
47	Y-08-01	55615.46	$0.739^{\pm0.078}$	$0.250^{\pm0.048}$	$0.338^{\pm0.101}$	$75.74^{\pm7.360}$	$1.311^{\pm0.048}$	$41.59^{\pm5.565}$	$1.311^{\pm0.112}$	$0.978^{\pm0.201}$	–	–	–	45.31/45
48	Y-09-00	55617.55	$0.680^{\pm0.038}$	$0.181^{\pm0.025}$	$0.266^{\pm0.052}$	$86.00^{\pm8.680}$	$1.330^{\pm0.033}$	$47.95^{\pm6.030}$	$1.188^{\pm0.089}$	$1.168^{\pm0.148}$	–	–	–	35.24/45
49	Y-09-02	55622.48	$0.628^{\pm0.038}$	$0.149^{\pm0.021}$	$0.237^{\pm0.048}$	$107.5^{\pm10.21}$	$1.399^{\pm0.040}$	$62.66^{\pm7.743}$	$1.036^{\pm0.079}$	$1.140^{\pm0.203}$	–	–	–	29.40/45
50	Y-10-01	55626.55	$0.609^{\pm0.048}$	$0.136^{\pm0.089}$	$0.223^{\pm0.164}$	$133.6^{\pm14.92}$	$1.413^{\pm0.048}$	$78.45^{\pm11.43}$	$0.844^{\pm0.076}$	$1.175^{\pm0.218}$	–	–	–	27.61/45

Here X=95409-01, Y=96409-01 mean the initial part of the observation Ids, and (a-f) mark TCAF model fitted results for six different states, presented in Fig. 4.
Intermediate horizontal lines mark state transitions from HS→HIMS, HIMS→SIMS, SIMS→SS, SS→SIMS, SIMS→HIMS, and HIMS→HS respectively.
$\dot{m}_h$, and $\dot{m}_d$ represent TCAF model fitted sub-Keplerian (halo) and Keplerian (disk) rates in Eddington rate respectively. X_s (in Schwarzschild radius r_g), and
R are the model fitted shock location and compression ratio values respectively. h_{shk} (in r_g) and T_{shk} (in 10^{10} K) are the shock height and temperature values
derived from Eqs. 4 & 5 respectively. R_z (in km) represents effective height of the Keplerian component at the pre-shock region.
$\dagger$ LW and LD represent Gaussian model fitted Iron line ($\sim 6.2 - 6.7$ keV) width and depth respectively.
$\dagger\dagger$ Here, frequencies of the principal QPO in Hz are presented. DOF means degrees of freedom of the model fit.